BIOLOGICAL OPTICS

The image-forming mirror in the eye of the scallop

Benjamin A. Palmer,[1]*† Gavin J. Taylor,[2]* Vlad Brumfeld,[3] Dvir Gur,[4,5] Michal Shemesh,[1,4] Nadav Elad,[3] Aya Osherov,[1] Dan Oron,[5] Steve Weiner,[1] Lia Addadi[1]†

Scallops possess a visual system comprising up to 200 eyes, each containing a concave mirror rather than a lens to focus light. The hierarchical organization of the multilayered mirror is controlled for image formation, from the component guanine crystals at the nanoscale to the complex three-dimensional morphology at the millimeter level. The layered structure of the mirror is tuned to reflect the wavelengths of light penetrating the scallop's habitat and is tiled with a mosaic of square guanine crystals, which reduces optical aberrations. The mirror forms images on a double-layered retina used for separately imaging the peripheral and central fields of view. The tiled, off-axis mirror of the scallop eye bears a striking resemblance to the segmented mirrors of reflecting telescopes.

In some rare visual systems in nature, mirrors are used instead of lenses to produce images (*1*). A remarkable example of such an eye is found in the *Pecten* scallop, which possesses up to 200 minute eyes lining the mantle tissue (Fig. 1, A and B). For more than two centuries, this peculiar feature of scallops fascinated scientists (*2*), but it was not until the 1960s that the image-forming mechanism was discovered. In seminal work, Land (*3*) showed that an image is formed when light is reflected off a concave mirror at the back of the eye onto the retina residing above it (Fig. 1, C and D). Similar eyes have since been found in crustaceans (*4*) and deep sea fish (*5*, *6*). In the *Pecten* scallop, each eye is ~1 mm in diameter (Fig. 1B) and is composed of a cornea, a weakly refracting lens, and a concave mirror, in addition to a highly unusual double-layered retina (Fig. 1, C and D). The upper (distal) retina is composed of ciliated photoreceptor bodies and resembles a vertebrate photoreceptor, whereas the lower (proximal) retina is composed of microvilli and is similar to the photoreceptor cells of other invertebrates (*7*). Calculations show that a simple spherical mirror would have its focal point in the distal retina (*3*), suggesting that only the distal retina is involved in image formation.

Land determined that the scallop mirror is a multilayer reflector and suggested that crystalline guanine was the functional optical material (*8*). However, the fragile tissue could not be preserved during transmission electron microscopy (TEM) preparation procedures, in which dehydration resulted in the loss of the crystals and collapse of the cytoplasm. Mirrors in nature are often constructed from alternating layers of materials with different refractive indices so that light reflected from the different layers undergoes constructive interference for some wavelengths and destructive interference for others. Many natural photonic systems use guanine crystals and cytoplasm as the high- and low-refractive-index materials (*9*–*11*), respectively, producing an extraordinary array of optical phenomena, from the white color in certain spiders (*12*) to the silvery reflectance of fish scales (*13*–*16*) and the brilliant iridescent colors of planktonic crustaceans (*17*, *18*) and tropical fish (*19*).

Perhaps the most complex optical function of guanine crystals in nature is in image formation. This function demands an extremely high degree of ultrastructural organization because light must not only be reflected but also focused. The hierarchal organization of the scallop mirror is finely tuned for image formation, from the component guanine crystals at the nanoscale to the overall shape of the mirror at the millimeter level (*20*). The scallop controls the crystal morphology and spacing to produce a tiled multilayer mirror with minimal optical diffraction aberrations, which reflects wavelengths of light that penetrate its habitat and are absorbed by its retinas. The mirror forms functional images on both retinas, which appear to be specialized for different functions.

Using cryogenic scanning electron microscopy (cryo-SEM), we imaged the ultrastructural properties of the mirror of the scallop *Pecten maximus* in close-to-physiological conditions, retaining the crystals and the cytoplasm spacings. The multilayered mirror is constructed from 20 to 30 layers of crystals separated by thin layers of cytoplasm (Fig. 2A). Each layer is composed of a tiling of closely packed crystal plates (Fig. 2B), which are organized so that each square, micron-wide crystal (Fig. 2, B to D) lies directly beneath a crystal in an adjacent layer, forming a vertical stack (Fig. 2C). The crystals are monodisperse, and the morphology is highly conserved, suggesting that crystal growth is strongly controlled.

The key to the functionality of the mirror lies in the regular square {100} plates of β-guanine, which constitute the mirror's basic building blocks. This unusual square morphology differs markedly from the theoretically predicted prismatic growth form of guanine. In this morphology, the crystal face with the highest refractive index (n = 1.83) is preferentially expressed, as is also the case in many other highly reflective natural photonic systems (*11*). The crystals are arranged so that the high-refractive-index faces are oriented toward the direction of the incident light across the mirror (fig. S1), creating a highly reflective surface. The square-plate morphology is also optimized for tiling. Each layer of the mirror is formed from an almost perfectly tessellated mosaic of two-dimensional (2D) squares—closely resembling the segmented mirrors used in reflecting telescopes (*21*). In Euclidean geometry, there are only three possible ways to completely tile a surface using regular congruent polygons: with equilateral triangles, with hexagons, or with squares (*22*). Crystal tiling minimizes surface defects at the crystal interfaces that would cause optical diffraction effects (which would result in a reduction in the image contrast) and optical loss owing to transmission of light through the mirror. Thus, at the lowest hierarchical level of organization, the scallop controls crystal growth to produce a crystal morphology that minimizes surface defects in the mirror and enables the formation of a highly reflective surface.

The guanine crystals have an average thickness of 74 ± 9 nm (N = 100) and an average cytoplasm spacing of 86 ± 18 nm (N = 96) (means ± SD), as measured from high-resolution cryo-SEM micrographs (Fig. 3A). With these data, the simulated reflectance spectrum obtained using a Monte Carlo transfer matrix calculation (*20*) reveals a peak in the blue/green at 500 nm approaching unity reflection, which closely matches the measured reflectivity spectrum that we recorded on whole *P. maximus* eyes (Fig. 3B). This peak is also coincident with the absorption maxima of the photoreceptors in the two retinas, which range between 475 and 540 nm (*23*, *24*), and with the peak in the irradiance spectrum of light that penetrates the scallop's habitat (Fig. 3B). Thus, at this hierarchal level of organization, the layer structure of the mirror is highly controlled and is well suited to reflect nearly all the blue/green light that penetrates the scallop's habitat at a wavelength range that is effectively absorbed by the photoreceptors of both retinas.

X-ray micro–computed tomography (micro-CT) measurements were performed on both fresh (fig. S2) and chemically fixed (Fig. 4, fig. S3, and movie S1) *P. maximus* eyes to determine the 3D morphology of the mirror and the organization of the eye components on a length scale of microns to millimeters. Three regions of high x-ray attenuation were identified in the eye, corresponding to the cornea, "iris" (an area of pigmented epithelial cells), and mirror, whereas the weakly absorbing lens body is located centrally (Fig. 4, A and B). Two striking features were observed in all the eyes. First, the mirror

[1]Department of Structural Biology, Weizmann Institute of Science, Rehovot 7610001, Israel. [2]Department of Biology, Lund University, Lund 22362, Sweden. [3]Department of Chemical Research Support, Weizmann Institute of Science, Rehovot 7610001, Israel. [4]Department of Molecular Cell Biology, Weizmann Institute of Science, Rehovot 7610001, Israel. [5]Department of Physics of Complex Systems, Weizmann Institute of Science, Rehovot 7610001, Israel.
*These authors contributed equally to this work.
†Corresponding author. Email: benjamin.palmer@weizmann.ac.il (B.A.P.); lia.addadi@weizmann.ac.il (L.A.)

does not have a simple hemispherical shape. Rather, the curvature of the mirror varies across its surface and is lowest at its base, which is typically flattened (Fig. 4, A to C, and figs. S2 to S4). Second, the optical axes of the mirror and the lens are not aligned (Fig. 4B); the eye has an off-axis optical configuration (*5*, *6*). Using the 3D eye geometry segmented directly from micro-CT volumes, we performed optical ray-tracing simulations (supplementary materials). Simulations (Fig. 4C and fig. S5) show that on-axis light reflected from the mirror is focused in the area occupied by the distal and proximal retinas (Fig. 1C and figs. S6 to S8), with light from off-axis sources best focused within the proximal retina (Fig. 4C). Further simulations of light from point sources across the eye's field of view (which subtends a full angle of ~120°) predict that images would be formed in a region of the distal retina viewing the upper visual field, whereas the proximal retina would have a better view of the lower visual field (Fig. 4D and fig. S10B). The best image formed on the proximal retina is at the periphery of the field of view (yellow spot, Fig. 4D), whereas the best image on the distal retina is formed just above the central field of view (red spot, Fig. 4D). Two-dimensional ray-tracing calculations (fig. S5) performed on a profile of the mirror from a fresh scallop eye (*20*) show that as the angle of incidence increases, the position of the focal point above the surface of the mirror changes. Whereas light is initially focused at the height of the distal retina (from 0° to 20°; figs. S7 and S8), the focal point moves progressively toward the lower proximal retina at higher incidence angles (40° to 60°). Although both retinas suffer from obvious spherical aberration and astigmatism (primarily resulting from the irregular curvature of the mirror), different regions on both retinas obtain angular resolutions of ~5° (*25*, *26*) (Fig. 4, D and E, and figs. S9 and S11). The nonspherical symmetry and tilt of the mirror produce more complex vision than was previously imagined: A simple on-axis, spherical mirror would not result in opposite sides of the visual field being focused as distinctly separate images at different heights above the mirror.

The direct consequence of the complex 3D morphology of the eye is that images are formed on both the distal and proximal retinas. Previous studies (*27*, *28*) showed that the distal retina responds to relatively dark, moving features, triggering defense or escape reflexes. Yet the role of the underlying, larger proximal retina remained enigmatic (*3*, *29*, *30*). The best-resolved image formed on the proximal retina is at the periphery of the visual field (extending ~30° to ~50° away from the visual axis). We suggest that the scallop's well-focused peripheral vision could provide useful information to control and guide its movement while swimming with jet propulsion or to assess static features of its habitat (*3*, *8*). Electrophysiology studies (*31*) determined that the proximal retina responded more slowly, but was considerably more sensitive, than the distal retina. We find that light focused onto the periphery of the eye (fig. S10) is substantially less intense than on-axis light, suggesting that the light-sensitive proximal retina is adapted for transduction when poorly illuminated. The task-specific functions of the scallop's distal and proximal retinas are reminiscent of the specialized retinal regions that occur in other animals, such as the dorsal rim areas used by insects for polarization detection (*32*) or the tiered photoreceptor layers in the mid-band rows used by stomatopods for color vision (*33*). There is also a striking correspondence between the apparent functions of the scallop's

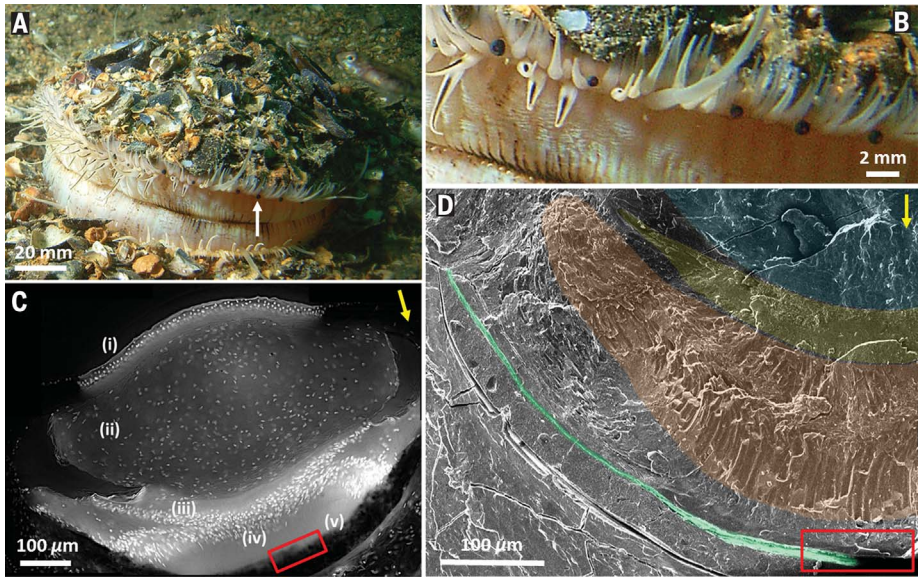

Fig. 1. The locations and anatomy of scallop eyes. (**A**) The scallop *Pecten maximus* with numerous eyes lining the mantle (the white arrow points to an individual eye). (**B**) A magnified image of five eyes. (**C**) Fluorescence microscopy image of an eye cross section, showing the cell nuclei stained with DAPI (4′,6-diamidino-2-phenylindole). The (i) cornea, (ii) lens, (iii) distal retina, (iv) proximal retina, and (v) concave mirror are indicated. (**D**) Low-resolution cryo-SEM micrograph of an eye cross section after high-pressure freezing and freeze-fracturing. The lens (blue), distal retina (yellow), proximal retina (orange), and concave mirror (green) are shown in pseudo-colors. The cilia and microvilli of the photoreceptors were used to identify the locations of the distal and proximal retinas. Red boxes in (C) and (D) identify the region of the central mirror explored in more detail in Fig. 2. Yellow arrows in (C) and (D), direction of on-axis incident light.

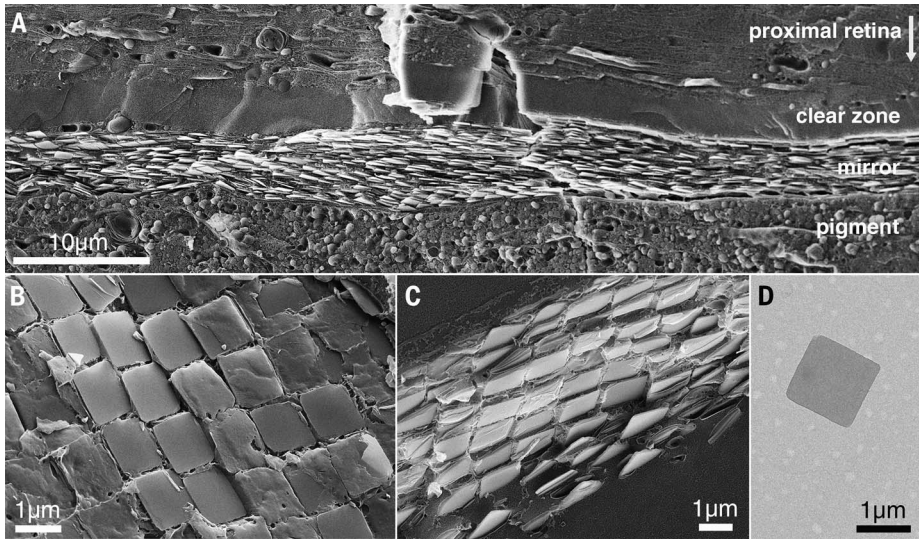

Fig. 2. The ultrastructure of the multilayer mirror. (**A** to **C**) Cryo-SEM micrographs of high-pressure–frozen, freeze-fractured cross sections through the eye of *P. maximus*. (A) The mirror viewed perpendicular to the eye axis. White arrow, direction of on-axis incident light. (B) The tiled mirror viewed from above. (C) Crystals in adjacent layers, stacked directly on top of one another, viewed in a fracture through the mirror. (**D**) TEM micrograph of a single, regular square crystal extracted from the eye. The crystals are 1.23 × 1.23 ± 0.08 μm (N = 20) with internal corner angles of 90.16 ± 2.78° (N = 28) (means ± SD).

distal and proximal retinas and the cone and rod cells of mammals. The light-sensitive rod cells of mammals are distributed at the outer edges of the retina and are specialized for peripheral vision in dim light and thus function analogously to the photoreceptors of the scallop's proximal retina. Mammalian cone cells located at the center of the retina are relatively less sensitive and respond rapidly to visual changes, functioning analogously to the distal retina of the scallop. Although multilayered retinas have infrequently been observed in other animals (*34*–*36*), in these cases, they are used to enhance light sensitivity or act as spectral filters (*37*). In contrast, in the scallop, the upper and lower parts of the retina seem to be specialized for discriminating different fields of view. Thus, at the highest hierarchical level of organization, the complex 3D shape of the scallop eye mirror appears to be controlled to focus light from a broad field of view onto two retinas placed at different heights above its surface.

What benefit does the scallop receive by having up to 200 eyes located on the periphery of its semi-circular mantle, spanning ~250°? Ray tracing reveals that the images formed on both retinas of one eye vary substantially in focal quality across their visual fields. Interestingly, the optic nerves from nearly all of the eyes project on to the lateral lobes of the parieto-visceral ganglion (PVG), the site of visual processing in scallops (*38*). We speculate that neural processing in the PVG can combine the visual information from the

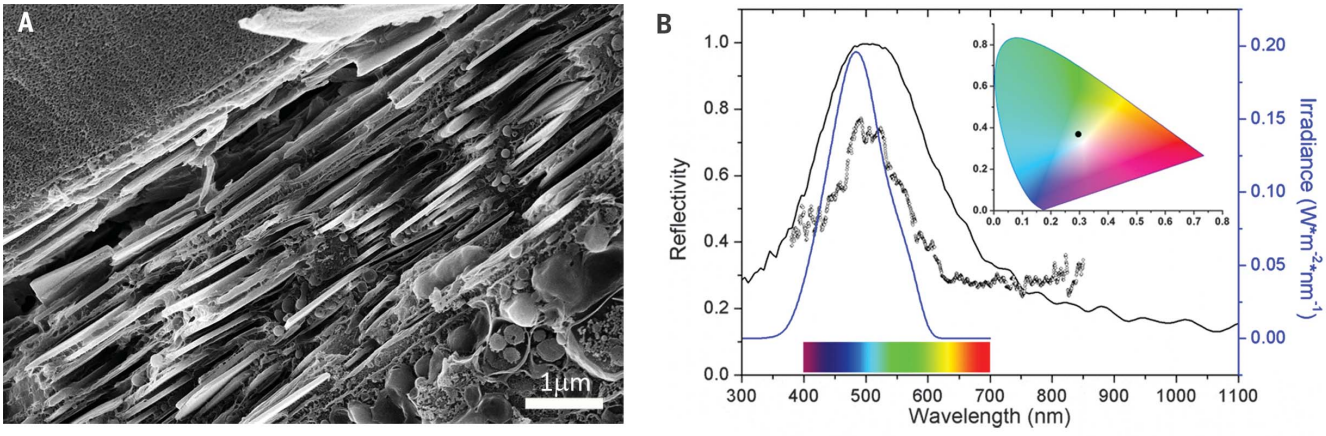

Fig. 3. The reflectivity of the mirror. (**A**) Cryo-SEM micrograph of the multilayer mirror, showing the crystal stacking. (**B**) Simulated (solid black trace) and measured (dotted black trace) reflectivity spectra overlaid with the calculated irradiance spectrum (blue trace) at a depth of 20 m in the scallop's habitat (*20*). The inset shows the mirror color (black dot) on a CIE (International Commission on Illumination) chromaticity space diagram. The reduced intensity in the measured reflectivity (which reaches a maximum of 75% at 500 nm) is caused by absorption and scattering processes within the optical path through the eye. The optical path involves passing light through the cornea, lens, and retina before it is reflected off the mirror and back through these elements to the detector.

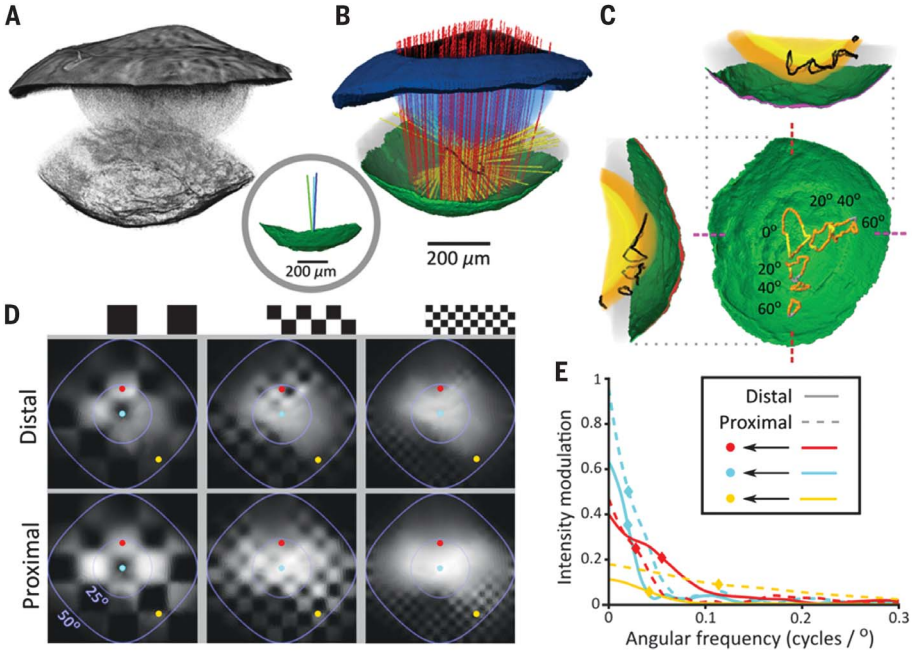

Fig. 4. Whole-eye optics. (**A**) Volume rendering of an x-ray micro-CT scan of a whole scallop eye, showing the eye anatomy. (**B**) Segmentation of the micro-CT in (A). Black, cornea; navy, "iris;" blue, lens; gray, gross retinal volume; green, mirror. Rays traced through the eye from a point source aligned with the axis of the lens (red) are reflected (yellow) and focused on the retina. The border of the best-focused region encompassing all reflected rays denotes a 3D circle of least confusion (COLC; black line). The inset is a side view of the mirror showing the optical axes of the lens (blue), central mirror (green), and center of the visual field (cyan). The lens and mirror axes are offset by 7.3°. (**C**) Top and side views of COLCs from sources consecutively offset by 20° from the original point source in (B), labeled 0°. The colors of the COLCs indicate which retina the COLCs pass through: yellow, distal; orange, proximal. (**D**) Simulated retinal images of planar checkerboards displaying increasingly finer details, corresponding to angular periods of 40°, 20°, and 10° (from left to right) (*26*). The purple borders in the images denote the extent of different visual angles. Red and yellow spots denote the positions of the best images formed on the distal and proximal retinas, respectively; cyan spots denote the center of each image. (**E**) The modulation transfer functions of the optics (figs. S9 and S10), calculated on both retinal surfaces at the colored spots in (D), indicate how different angular frequencies (*26*) are modulated in the resulting image on the retina. Diamonds label the points at which the curves are reduced to 50% of the local zero-frequency intensity (the cut-off frequency).

substantially overlapping and differently focused views from multiple eyes, allowing the scallop to improve visual acuity relative to the isolated eye and potentially to determine the depth of features in the environment. This would offset the drawback of limited areas of well-focused vision in individual eyes.

The crystal morphology, multilayer structure, and 3D shape of the scallop's eye mirror are finely controlled to produce functional images on its two retinas. Understanding the strategies that organisms use to control crystal morphology and arrangement for complex optical functions paves the way for the construction of novel bio-inspired optical devices (*39*, *40*). In particular, the resemblance of the scallop's tiled, off-axis mirror to the segmented mirrors of reflecting telescopes provides inspiration for the development of compact, wide-field imaging devices derived from this unusual form of biological optics.

REFERENCES AND NOTES

1. M. F. Land, D.-E. Nilsson, *Animal Eyes* (Oxford Univ. Press, 2012).
2. I. X. Poli, *Testacea utriusque Siciliae eorumque historia et anatome*, tome 2 (1795).
3. M. F. Land, *J. Physiol.* **179**, 138–153 (1965).
4. A. Andersson, D.-E. Nilsson, *Protoplasma* **107**, 361–374 (1981).
5. H.-J. Wagner, R. H. Douglas, T. M. Frank, N. W. Roberts, J. C. Partridge, *Curr. Biol.* **19**, 108–114 (2009).
6. J. C. Partridge *et al*., *Proc. Biol. Sci.* **281**, 20133223 (2014).
7. V. C. Barber, E. M. Evans, M. F. Land, *Z. Zellforsch. Mikrosk. Anat.* **76**, 25–312 (1967).
8. M. F. Land, *J. Exp. Biol.* **45**, 433–447 (1966).
9. T. M. Jordan, J. C. Partridge, N. W. Roberts, *J. R. Soc. Interface* **11**, 20140948 (2014).
10. J. Teyssier, S. V. Saenko, D. van der Marel, M. C. Milinkovitch, *Nat. Commun.* **6**, 6368–6375 (2015).
11. D. Gur, B. A. Palmer, S. Weiner, L. Addadi, *Adv. Funct. Mater.* **27**, 1603514 (2017).
12. A. Levy-Lior *et al*., *Adv. Funct. Mater.* **20**, 320–329 (2010).
13. E. J. Denton, M. F. Land, *Proc. R. Soc. Lond. B Biol. Sci.* **178**, 43–61 (1971).
14. A. Levy-Lior *et al*., *Cryst. Growth Des.* **8**, 507–511 (2008).
15. D. Gur, B. Leshem, D. Oron, S. Weiner, L. Addadi, *J. Am. Chem. Soc.* **136**, 17236–17242 (2014).
16. T. M. Jordan, J. C. Partridge, N. W. Roberts, *Nat. Photonics* **6**, 759–763 (2012).
17. D. Gur *et al*., *J. Am. Chem. Soc.* **137**, 8408–8411 (2015).
18. D. Gur *et al*., *Adv. Funct. Mater.* **26**, 1393–1399 (2016).
19. D. Gur *et al*., *Angew. Chem. Int. Ed.* **54**, 12426–12430 (2015).
20. Materials and methods are available as supplementary materials.
21. W. P. McCray, *Giant Telescopes* (Harvard Univ. Press, 2006).
22. J. Kepler, *Harmonices Mundi* (1619).
23. J. R. Cronly-Dillon, *Science* **151**, 345–346 (1966).
24. D. I. Speiser, E. R. Loew, S. Johnsen, *J. Exp. Biol.* **214**, 422–431 (2011).
25. The angular resolution defines the resolution limit of the eye and is the minimum angle subtended between two points in space that will be resolved as separate images on the retina. In this case, individual features (i.e., a single black square, or half the angular period of a checkerboard) are resolvable at angles of ~5°. Our results agree well with previous behavioral studies (*29*, *30*). The angular resolution for a similarly sized diffraction-limited optical system is 0.065°.
26. The angular period is defined as the angle subtended between identical features of the object (i.e., between two black squares in the checkerboard). Angular period = 1/angular frequency.
27. M. F. Land, *J. Exp. Biol.* **45**, 83–99 (1966).
28. D. I. Speiser, S. Johnsen, *J. Exp. Biol.* **211**, 2066–2070 (2008).
29. D. I. Speiser, D. Johnsen, *Am. Malacol. Bull.* **26**, 27–33 (2008).
30. D. I. Speiser, Y. L. Gagnon, R. K. Chhetri, A. L. Oldenburg, S. Johnsen, *Integr. Comp. Biol.* **56**, 796–808 (2016).
31. J. S. McReynolds, A. L. F. Gorman, *J. Gen. Physiol.* **56**, 376–391 (1970).
32. U. Homberg, A. Paech, *Arthropod Struct. Dev.* **30**, 271–280 (2002).
33. J. Marshall, T. W. Cronin, S. Kleinlogel, *Arthropod Struct. Dev.* **36**, 420–448 (2007).
34. M. F. Land, *J. Exp. Biol.* **51**, 471–493 (1969).
35. M. Michinomae, H. Masuda, M. Seidou, Y. Kito, *J. Exp. Biol.* **193**, 1–12 (1994).
36. E. Denton, N. A. Locket, *J. Mar. Biol. Assoc. U. K.* **69**, 409–435 (1989).
37. E. J. Warrant, N. A. Locket, *Biol. Rev. Camb. Philos. Soc.* **79**, 671–712 (2004).
38. T. Spagnolia, L. A. Wilkens, *Mar. Behav. Physiol.* **10**, 23–55 (1983).
39. L. Li *et al*., *Science* **350**, 952–956 (2015).
40. K. H. Jeong, J. Kim, L. P. Lee, *Science* **312**, 557–561 (2006).

ACKNOWLEDGMENTS

We thank C. Jones of Haven Diving Services for supplying the scallops and for the photographs in Fig. 1, A and B, and A. Hirsch for her help in the analysis of TEM images. We thank B. Geiger for the use of DeltaVision fluorescence microscopy. Electron microscopy studies were supported by the Irving and Cherna Moskowitz Center for Nano and Bio-Nano Imaging at the Weizmann Institute of Science. This work was supported by the Israel Science Foundation (grant 2012\224330*), the Crown Center of Photonics, and the I-CORE (Israeli Center for Research Excellence) "Circle of Light." B.A.P. is the recipient of a Human Frontiers Cross-Disciplinary Postdoctoral Fellowship. G.J.T. is supported by a stipend from Carl Tryggers Stiftelse (CTS15:38). L.A. and S.W. are the incumbents of the Dorothy and Patrick Gorman Professorial Chair of Biological Ultrastructure and the Dr. Trude Burchardt Professorial Chair of Structural Biology, respectively.

SUPPLEMENTARY MATERIALS

www.sciencemag.org/content/358/6367/1172/suppl/DC1
Materials and Methods
Figs. S1 to S11
References (*41*–*48*)
Movie S1

9 February 2017; resubmitted 25 June 2017
Accepted 23 October 2017
10.1126/science.aam9506